Increased nanoparticle penetration in collagenase-treated multicellular spheroids

Thomas T Goodman[1]
Peggy L Olive[2]
Suzie H Pun[1]

[1]Department of Bioengineering, University of Washington, Seattle, WA, USA; [2]BC Cancer Research Centre, Vancouver, BC, Canada

Abstract: The extracellular matrix of solid tumors presents a transport barrier that restricts nanoparticle penetration, thereby limiting the efficacy of nano-sized delivery vehicles for cancer imaging and therapy. In this study, the effect of nanoparticle size and collagenase treatment on penetration of carboxylated polystyrene nanoparticles was systematically assessed in a multicellular spheroid model. Penetration of the nanoparticles into the spheroid core was limited to particles smaller than 100 nm. Collagenase treatment of spheroids resulted in significantly increased penetration of nanoparticles up to 100 nm with only a minor increase in particle penetration observed for particles larger than 100 nm. Collagenase was immobilized onto the surface of nanoparticles for site-specific degradation of ECM proteins. Collagenase-coated, 100 nm nanoparticles demonstrated a 4-fold increase in the number of particles delivered to the spheroid core compared with control nanoparticles. Thus, nanoparticle delivery to solid tumors may be substantially improved by the incorporation of ECM-modulating enzymes in the delivery formulation.

Keywords: nanoparticles, collagenase, cancer treatment, spheroids, solid tumors

Introduction

Nanoparticulate delivery vehicles such as polymer-small molecule conjugates, liposomes, and viruses offer distinct advantages for anti-cancer treatment approaches, including selective accumulation in tumor areas due to the enhanced permeability and retention (EPR) effect, cocktail packaging of molecular imaging and therapeutic agents, and delivery of macromolecules such as nucleic acids and proteins. Typical sizes of nanoparticles being developed for clinical applications range from 2 nm to 200 nm (Portney and Ozkan 2006). Effective treatment of solid tumors requires that the nanoparticles reach as many cells within the tumor as possible, but penetration into tumor tissue is a significant problem for relatively large particles such as liposomes and viruses that are directly injected in solid tumors (Pluen et al 2001; Grill et al 2002; Kostarelos et al 2004).

The limited spread of nanoparticles in solid tumors following extravasation can be attributed to binding within tumor tissue, increased interstitial fluid pressure caused by leaky vasculature and poor lymphatic drainage, and torturosity and hindered diffusion due to cell packing and the extracellular matrix (ECM) (Netti et al 2000; Jain 2001; Kuppen et al 2001; Davies et al 2001; Grantab et al 2006). To minimize the "binding site barrier", nanoparticles can be surface-modified with non-fouling materials such as polyethylene glycol to reduce this non-specific binding (Kaul and Amiji 2005). Previous work has demonstrated that eliminating the pressure gradient within solid tumors results in minimal enhancement in macromolecule delivery suggesting that high interstitial pressure within solid tumors is not the only major barrier to penetration of macromolecules (Flessner et al 2005). Several recent studies

Correspondence: Suzie H Pun
University of Washington, Department of Bioengineering, Box 355061, Seattle, WA 98195, USA
Tel +1 206 685 3488
Email spun@u.washington.edu

© 2007 Dove Medical Press Limited. All rights reserved

reveal that the ECM provides a major barrier to antibody penetration in solid tumors (Netti et al 2000; Davies et al 2002; Choi et al 2006). Modulation of the ECM by intravenous injection of protease enzymes into xenograft tumors increases the spread of macromolecules such as antibodies, and direct injection of protease enzymes increases the penetration of nanoparticles such as viruses administered to the tumor (Eikenes et al 2004; McKee et al 2006). The relative effect of various components of the ECM most likely varies with tumor type, as ECM differs among tumors of different type and location (Pluen et al 2001), but several studies have shown that collagenase improves macromolecular penetration depth (Kuriyama et al 2001; Alexandrakis et al 2004; Eikenes et al 2004; Choi et al 2006; McKee et al 2006), while treatment with hyaluronidase yielded mixed results (Alexandrakis et al 2004; Eikenes et al 2005; Choi et al 2006). These in vivo studies demonstrate that disruption of the ECM can significantly improve the efficacy of several therapeutic systems in solid tumors. However, the applicability of this approach to the broad class of nanoparticulate delivery vehicles is not yet clear.

The goal of this work was to investigate the effects of nanoparticle size and ECM integrity on nanoparticle penetration. The diffusion in collagen gels and solid tumors of macromolecules that are typically an order of magnitude smaller than nanoparticles used for drug delivery has been studied using high molecular weight dextrans and proteins as tracer molecules (Ramanujan et al 2002; Alexandrakis et al 2004; Dreher et al 2006). However, the limitations of nanoparticle penetration have not yet been systematically assessed. In this study, penetration of model nanoparticles ranging from 20 to 200 nm in diameter was assessed in a three-dimensional, multicellular spheroid tumor model. Multicellular spheroids (MCS) are cultured cells grown in a three-dimensional, spherical arrangement and provide tissue-like cell-cell interactions and extracellular matrix production (Sutherland 1988). In addition, the effect of ECM modulation on nanoparticle penetration in spheroids was investigated. Treatment of spheroids with collagenase either in solution or immobilized on the nanoparticle surface resulted in significantly increased nanoparticle penetration.

Materials and methods

Cell culture and multicellular spheroid formation

Cell culture media, serum, and supplements were purchased from Mediatech (Herndon, VA). SiHa (human cervical carcinoma) cells were maintained in monolayer cultures prior to spheroid formation. To initiate spheroid growth, monolayer cells were trypsinized, and 10^7 cells were added to a 250 ml spinner flask (Belco, Vineland, NJ) containing 200 ml complete media (MEM media with 10% FBS and antibiotic-antimytotic solution) that was pre-equilibrated to 5% CO_2. Cells were stirred in the sealed spinner flask at 150 RPM in an incubator at 37 °C. After 3 days, 150 ml of media was removed from the spinner flask and replaced with 150 ml of fresh media. The media was then replaced daily with 150 ml MEM containing 5% FBS and antibiotics.

Nanoparticle characterization

The sizes of fluorescently-labeled, carboxylated, 20, 40, 100, and 200 nm polystyrene beads (Invitrogen) were analyzed by dynamic light scattering (DLS) using a ZetaPALS analyzer (Brookhaven Instruments, Holtsville, NY) and by transmission electron microscopy (TEM). For TEM of polystyrene particles, 10 µl of bead stock solutions were spotted directly onto TEM grids, allowed to adsorb for 5 min followed by removal of residual fluid. To determine if particles aggregated under experimental conditions, particles were sized in deionized water and in OptiMEM, incubated for 3 h at 37 °C, and resized.

Nanoparticle delivery to multicellular spheroids

Spheroids with diameters between 400–500 µm were obtained after approximately 10–14 days of growth. For each experiment, ~30 spheroids were handpicked with a Pasteur pipette and transferred to a 1.5 ml siliconized tube. Media was exchanged to OptiMEM reduced serum media (Gibco, Grand Island, NY). Appropriate concentrations of collagenase (from *Clostridium histolyticum*, 0.74 U/mg, Sigma) were added to the spheroids followed by addition of fluorescently labeled polystyrene beads (Invitrogen, Carlsbad, CA). The beads were added to a final concentration of 7.58×10^{11} beads/ml for all sizes tested, and spheroids were rotated at 5 RPM for 5 h at 37 °C. The media was then removed by aspiration and spheroids were washed with phosphate buffered saline (pH 7.4) before further processing. For determination of relative nanoparticle concentrations in the outer cell layers compared with the core of the spheroids, the outer cell layers were removed from the spheroids using a procedure similar to that applied previously for sequential trypsinization of spheroids (Oloumi et al 2000). Spheroids were washed 3× with PBS + 2% FBS followed by the addition of 1 ml of 0.25% Trypsin or PBS (for controls). Spheroids were then

placed in a 12-well TC dish and rotated at 130 rpm for 20 min at 37 °C. Spheroids were imaged by epifluorescence microscopy to confirm that the outer cell layers were removed. The trypsin solution was aspirated off the spheroids and replaced with MEM + 10% FBS. The spheroids were transferred to 1.5 ml centrifuge tubes, washed twice with 1 ml PBS + 2% FBS, and resuspended in 300 µl PBS. The spheroids were broken up with vigorous pipetting and the solution was homogenized by sonicating 2× for 10 sec at 8–9 watts using a probe tip sonicator (Sonic Dismebrator 60, Fisher). The fluorescence of the sonicated cells was then measured by placing 250 µl of each sample in a 96-well plate and reading the fluorescence using a Tecan (Zurich, Switzerland) Safire^2 plate reader. The number of nanoparticles associated with the spheroid core (spheroids exposed to trypsin) and total spheroids (control spheroids exposed to PBS) was determined by comparison to a standard curve made by measuring fluorescence emission of nanoparticles prepared at known concentrations in cell lysate. The percentage of nanoparticles reaching the spheroid cores was determined by dividing the number of nanoparticles associated with trypsinized spheroid by the number of nanoparticles associated with spheroids that had not been exposed to trypsin.

Preparation and characterization of collagenase-coated nanoparticles

Polystyrene beads were coated with protein by incubating 75 µl of 100 nm bead stock (3.64×10^{14} beads/ml stock) with 375 µl of 5 mg/ml collagenase or albumin in H_2O for 12 hours. Beads were then sedimented by centrifugation at ~20,000 g and washed twice to remove free protein. Relative bead concentration was determined by measuring the fluorescence of each bead sample using a Safire^2 fluorimeter (Tecan, Research Triangle Park, NC) and comparing to a standard curve. The activity of the collagenase adsorbed to the bead surface was determined using a collagenase I assay kit following the manufacturer's instructions (Chemicon International, Temecula, CA; kit ECM710).

Fluorescence imaging and image analysis

For analysis of nanoparticle penetration by fluorescent imaging, spheroids were transferred to a cryomold, covered in optimal cutting temperature (O.C.T.) compound (Tissue-Tek, Torrance, CA), flash frozen in liquid nitrogen, and processed by cutting 8 µm sections using a CM1900 cryostat (Leica, Wetzlar, Germany). Fluorescent images of spheroid sections were obtained with a Nikon Eclipse TE2000-U inverted microscope (Meridian Instrument, Kent, WA) attached to a CoolSnapHQ CCD camera (Photometrics, Tucson, AZ) and analyzed using Metamorph software. To assess core fluorescence, individual images of spheroid sections were outlined manually and the outline of the spheroids was projected 40 µm into the spheroid using Metamorph. The integrated pixel intensity within the projected area was then normalized by spheroid area, and baseline fluorescence from spheroids not exposed to fluorescent beads was subtracted from the normalized signal. Samples were run in duplicate and at least five independent central spheroid sections were analyzed for each sample.

Flow cytometry

Cells were prepared for flow cytometry analysis by washing spheroids twice with PBS + 2% FBS and once with PBS followed by trypsinization with 0.25% trypsin in Hank's Balanced salt solution (HBSS) for 25 min at 37 °C. Trypsin was aspirated from the cells followed by two washes with PBS + 2% FBS, and propidium iodide was added to resuspended cells to a final concentration of 2 µg/ml. Cells were then analyzed using an LSR flow cytometer (BD Biosciences, San Jose, CA). For analysis, live cells were identified using forward and side scatter signal and then assessed for propidium iodide signal.

Immunostaining

Spheroid sections were stained for collagen using a polyclonal rabbit anti-human collagen antibody that was raised against collagens I-V (AbCam, Cambridge, MA; 1:100) and visualized with a AlexaFluor488 goat anti-rabbit IgG (H + L) secondary antibody (Invitrogen; 1:50). Cell nuclei were stained with a 1 µg/ml solution of DAPI for 30 min and sections were preserved using ProLong antifade solution (Invitrogen). Images of collagen stained samples were obtained using a Zeiss LSM 510 NLO inverted confocal microscope (NTUF University of Washington, Seattle, WA).

Transmission electron microscopy

Spheroid sections for TEM analysis were prepared by fixing spheroids in half strength Karnovsky's fixative (2% paraformaldehyde, 2.5% gluteraldehyde, 0.1 M cocadylate buffer, 3 mM $CaCl_2$, at pH 7.3) overnight followed by post fixing in 1.0% OsO_4 for 1 h. The spheroids were then stained with 2% uranyl acetate, rinsed and dehydrated with absolute ethanol and embedded in Eponate resin (Ted Pella, Redding CA). Sections were cut using a Reichert Ultracut E microtome and mounted on 150 mesh 0.25% formvar coated rhodium/copper grids. The sections were stained with uranyl acetate

and lead citrate and imaged with a JEM 1200EX II transmission electron microscope (JOEL Ltd, Tokyo, Japan). Tissue processing and imaging was performed at the University of Washington Pathology Electron Microscopy Resource Center (Seattle, WA).

Statistical analysis

Statistical analysis was performed using unpaired Students' t tests. Results were considered statistically significant with a p value <0.05.

Results

Particle size confirmation by DLS and TEM

The particle size of nanoparticles was determined by electron microscopy and light scattering analysis. Electron microscopy revealed that the 20 and 40 nm nanoparticles were more polydisperse than the 100 and 200 nm nanoparticles, but confirmed that four separate particle sizes were represented in these studies (Figure 1). Dynamic light scattering measurements of nanoparticles yielded mean diameters of 23.1 (±0.9) nm, 39.4 (±3.2) nm, 103.5 (±6.4) nm, and 209.0 (±35.4) nm for nanoparticles referred to hereafter as 20, 40, 100, and 200 nm respectively. The stability of nanoparticles under experimental conditions was assessed by incubation of the nanoparticles in OptiMEM for 3 hours followed by measurement of particle size. Light scattering measurements indicated that particles showed minor aggregation under experimental conditions, with an increase of 11.1 (±1.8)% in mean diameter for 200 nm particles, an 8.5 (±4.7)% increase for 100 nm particles and no significant change in size for 20 nm, and 40 nm particles after incubation in OptiMEM.

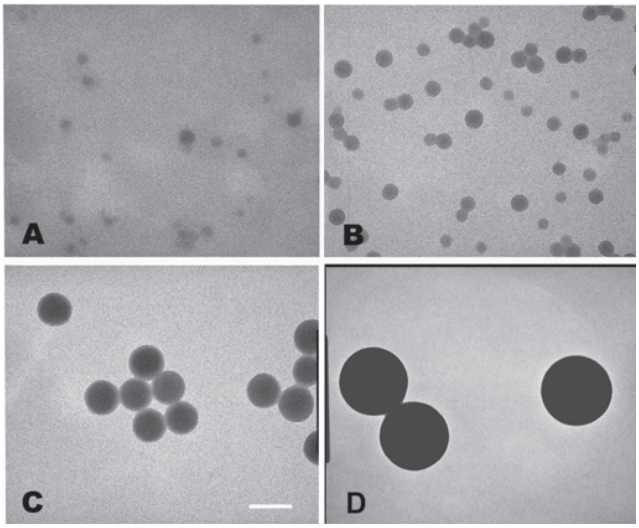

Figure 1 TEM images of polystyrene nanoparticles. Particle sizes shown are 20, 40, 100, and 200 nm (**A**–**D**, respectively). The scale bar represents 100 nm.

Optimizing collagenase concentration

The effect of ECM components on nanoparticle diffusion in tissue was assessed by degrading the fibrillar ECM protein, collagen, in multicellular spheroids (MCS) during exposure to nanoparticles. Spheroid integrity as a function of collagenase concentration was studied by microscopy. Treatment of spheroids with 0.1 mg/ml collagenase resulted in a slight loosening of cells at the outer spheroid perimeter, whereas treatment with 1.0 mg/ml of collagenase significantly affected spheroid architecture (Figure 2). Spheroids were also treated with various concentrations of collagenase along with 40 nm fluorescently labeled nanoparticles for 5 hours and particle penetration was analyzed by fluorescence microscopy and image analysis of sectioned spheroids. Nanoparticle penetration increased with collagenase concentration up to 0.5 mg/ml, with the first major increase in fluorescence occurring at a concentration of 0.1 mg/ml, where a 4-fold increase in nanoparticle fluorescence was observed (Figure 3). Collagenase-treated spheroids were also trypsinized to single-cell suspension and cell viability assessed by propidium iodide exclusion with flow cytometry analysis. No significant increase in propidium iodide signal was detected in the gated cell population with any samples treated with collagenase (up to 2.5 mg/ml collagenase; data not shown). Based on these studies, 0.1 mg/ml collagenase was determined to be the optimum collagenase concentration that impacts nanoparticle penetration without a concomitant loss of overall spheroid integrity and was used for subsequent studies with various sized nanoparticles.

Collagen staining and degradation of collagen by collagenase

In order to verify the presence of ECM in SiHa multicellular spheroids and the effect of collagenase treatment, spheroid sections were stained with antibodies that recognize collagens I-V and imaged by confocal microscopy. Collagen labeling confirmed significant collagen content in the SiHa multicellular spheroids (Figure 4A). Spheroids treated with 0.1 mg/ml of collagenase from *Clostridium histolyticum*, (0.74 U/mg), which cleaves human collagen types I, II, and III (Vanderrest et al 1977) resulted in a significant decrease in collagen content following collagenase treatment (Figure 4B). No signal was observed with controls without the primary collagen antibody (data not shown).

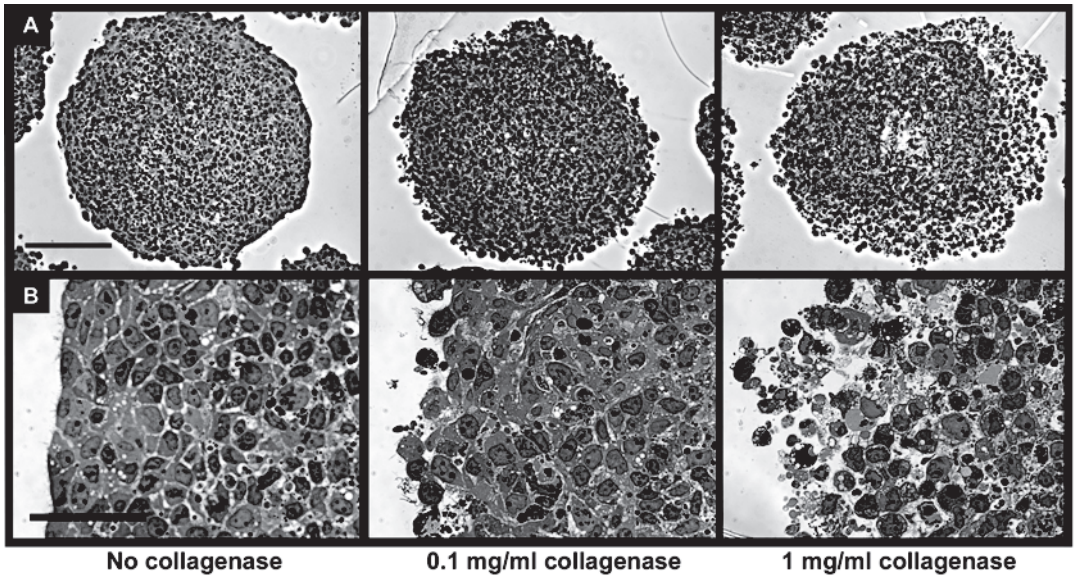

Figure 2 Optimization of collagenase concentration for nanoparticle delivery to multicellular spheroids. Brightfield images of spheroid integrity after collagenase treatment are shown in at low magnification (**A**, scale bar 150 μm) and high magnification (**B**, scale bar 50 μm). Images correspond to collagenase concentrations of 0, 0.1, and 1 mg/ml.

Effect of nanoparticle size on penetration in MCS

The effect of nanoparticle size on penetration in a three-dimensional cell culture model was assessed by incubating nanoparticles of various sizes (20, 40, 100, and 200 nm in diameter) with multicellular spheroids and quantifying particle association. Because a predominate percentage of the nanoparticles remain in the outer few cell layers, variations in fluorescence from these cells mask subtle changes in the penetration to the spheroid. Therefore, the penetration of nanoparticles into the "core" of untreated spheroids was investigated by removing the outer cell layers by gentle trypsinization of spheroids and analyzing the fluorescence remaining in the core of the spheroid. Fluorescence imaging of the spheroids before and after trypsination confirmed removal of the bright outer cell layers as well as the morphological integrity of the remaining spheroid core. The number of nanoparticles associated with the spheroids was determined by comparison to fluorescence standards made with cell lysates containing known nanoparticle concentrations. Results are shown as the percentage of nanoparticles in the spheroid core, calculated by dividing the number of nanoparticles associated with the spheroid cores by the number of nanoparticles in whole spheroids (without removal of outer cell layers). Our results show that the percentage of particles that enter the spheroid core decreases as particle size increase (Figure 5). The 20 nm and 40 nm nanoparticles penetrate effectively (57% and 32%, respectively, of spheroid-associated nanoparticles in the spheroid core) whereas 100 nm and 200 nm nanoparticles demonstrate restricted penetration (<5% of spheroid-associated nanoparticles in the spheroid core).

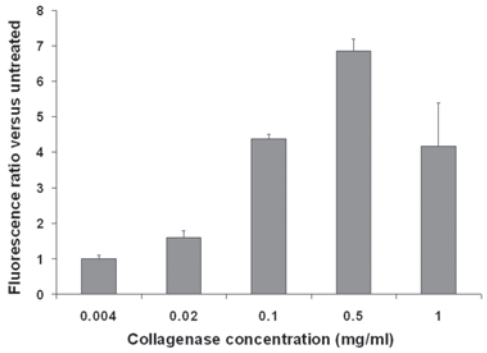

Figure 3 Quantification of nanoparticle association from spheroids co-incubated for 5 hours with 40 nm, fluorescently-labeled beads and various concentrations of collagenase are presented as the ratio of integrated spheroid section fluorescence compared with spheroids exposed to nanoparticles in the absence of collagenase treatment.

Effects of collagenase on nanoparticle penetration

The effect of collagen degradation on nanoparticle penetration was investigated by exposing the spheroids to fluorescently-labeled nanoparticles (20–200 nm in diameter) in the presence and absence of collagenase. Nanoparticle distributions in untreated spheroid cryosections are shown in Figure 6A (row 1). Some diffuse fluorescence is

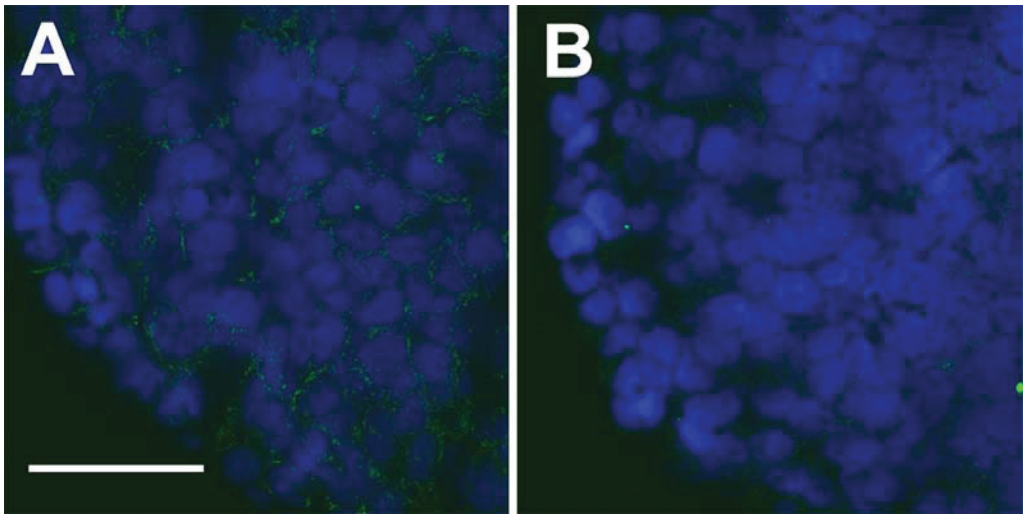

Figure 4 Collagen-stained spheroid cryosections in the untreated (**A**) and collagenase-treated (**B**) spheroids. Treated spheroids were exposed to 0.1 mg/ml of collagenase for 5 hours prior to sectioning and staining. Secondary antibody signal, indicating collagen staining, is shown in green and the nuclear stain, DAPI, is shown in blue. (Scale bar is 50 μm)

observed in the interior of spheroids exposed to 20 and 40 nm nanoparticles without collagenase, but nanoparticles were predominantly restricted to the spheroid periphery for all sizes. Collagenase treatment (0.1 mg/ml) of spheroids significantly increased the delivery of 20 nm and 40 nm nanoparticles to the MCS; nanoparticle fluorescence was clearly distributed throughout the treated spheroid sections (Figure 6A, row 2). A slight increase in fluorescence was observed with 100 nm and 200 nm nanoparticles following collagenase treatment but not to the extent of the smaller nanoparticles. No significant increase in cell autofluorescence was induced by collagenase treatment.

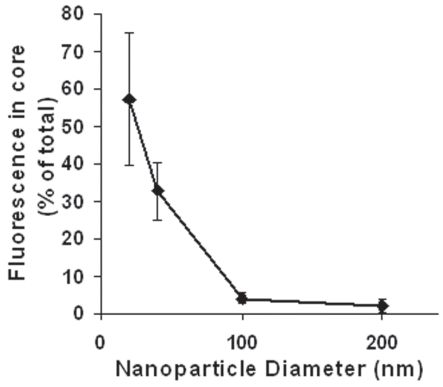

Figure 5 Percentage of spheroid-associated nanoparticles that penetrate past the outer few cell layers as a function of nanoparticle size. Spheroid cores were isolated by removing the outer cell layers of the spheroids with gentle trypsinization. The number of nanoparticles associated with the whole spheroids and spheroid cores was quantified by fluorescence measurements.

In order to quantify the effect of collagenase treatment on nanoparticle penetration, the fluorescence intensity of the spheroid sections was integrated using Metamorph software. Some cells from the outermost layers of the spheroid were likely dissociated from the spheroid following collagenase treatment. To eliminate contributions and variations from this outer layer, the core fluorescence per unit area was determined by integrating the fluorescence from the area of the spheroid up to the outer 40 μm rim and normalizing by the section area. It is also important to note that the measured fluorescence emission intensity per particle of the 40, 100, and 200 nm nanoparticles are 7-fold, 180-fold, and 1900-fold higher than the emission intensity of 20 nm nanoparticles, respectively. To adjust for this difference, the effect of collagenase treatment on nanoparticle penetration is reported as the ratio of the fluorescence per unit area of collagenase-treated spheroid sections to the fluorescence per unit area of untreated spheroid sections for each nanoparticle size. Collagenase treatment increased the penetration of 20 nm and 40 nm nanoparticles by 6.9 and 11.6 fold, respectively, while smaller effects were detected for the 100 nm and 200 nm nanoparticles (3.2- and 1.5-fold, respectively; Figure 6B).

TEM imaging of nanoparticle penetration

Sections of nanoparticle-treated spheroids were imaged by transmission electron microscopy in order to elucidate the mechanism of increased nanoparticle penetration. Electron micrographs revealed that SiHa cells are tightly packed in the spheroid, with many cells connected to neighboring cells via tight junctions. The 100 nm nanoparticles were easily

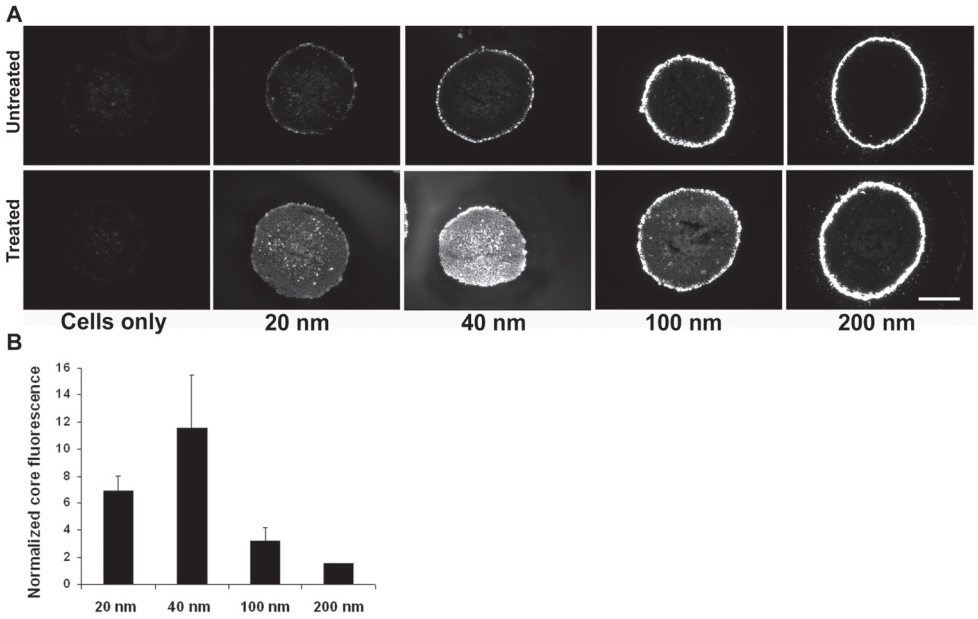

Figure 6. A. Fluorescence microscopy images of cryosections from spheroids co-incubated with various sizes of fluorescently-labeled nanoparticles with ("treated"), or without ("untreated") 0.1 mg/mL collagenase. Scale bar represents 200 μm. **B.** The ratio of integrated fluorescence from nanoparticles in the collagenase-treated versus untreated spheroid sections.

identifiable at high magnification by TEM and were found both in the intracellular and extracellular space (Figure 7). The extracellular particles were found mainly in paracellular gaps (Figure 7A) and at the surface of the spheroid (Figure 7B) while the intracellular particles were trapped in membrane bound vesicles (Figure 7C). The 40 nm nanoparticles were also observed in extracellular spaces between cells (not shown); however, internalized 40 nm nanoparticles and 20 nm nanoparticles were difficult to distinguish from cellular components by TEM.

Collagenase-coated nanoparticles exhibit improved penetration into spheroid tissue

There are several drawbacks to administration of free collagenase as an adjuvant to nanoparticle delivery. A more attractive option is the incorporation of active collagenase into the nanoparticle itself. A nanoparticle targeted to tumor tissue could mediate localized ECM degradation, thus reducing side effects from systemic or intratumoral collagenase delivery. In order to assess the effect of localized collagenase delivery, protein was adsorbed onto the nanoparticles by incubating the polystyrene nanoparticles with collagenase or albumin (as a control) solutions and removing free protein through multiple centrifugation washes. With this method, >99% of unadsorbed protein was removed.

To confirm that active collagenase was adsorbed on the nanoparticle surfaces, a colorimetric assay was used to quantify collagenase activity. The coated nanoparticles showed collagenase activity equivalent to ~0.33 μg/ml free collagenase, while no activity was observed with controls of BSA coated nanoparticles or nanoparticles alone. Incubation of spheroids with 100 nm collagenase-coated nanoparticles resulted in a significant increase (~4-fold) in spheroid core fluorescence compared with albumin-coated nanoparticles (Figure 8). There was no increase in core fluorescence when equivalent amounts of collagenase were added to albumin coated nanoparticles, where equivalent

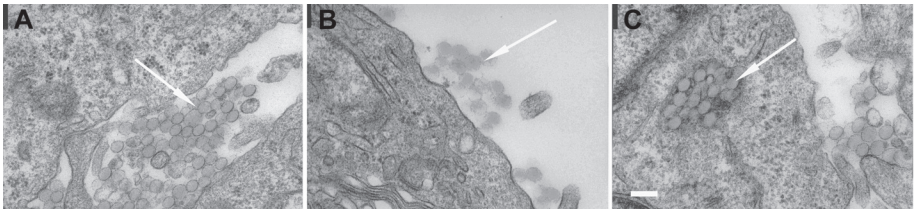

Figure 7. Representative TEM images of 100 nm nanoparticles in SiHa multicellular spheroid sections. Arrows indicate the location of the nanoparticles. The nanoparticles were found in the paracellular space (**A**), at the surface of the spheroids (**B**), and in intercellular vesicular structures (**C**). Bar = 200 nm.

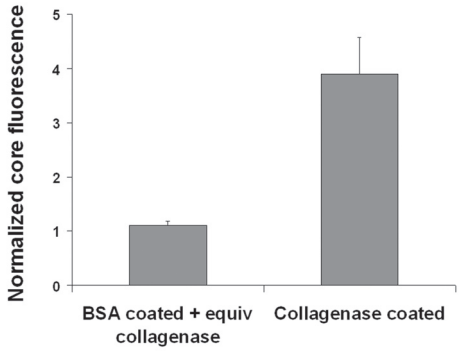

Figure 8. Penetration of collagenase-coated nanoparticles in multicellular spheroids. The penetration of collagenase-coated, 100 nm nanoparticles was quantified by image analysis of spheroid sections and normalized by the integrated fluorescence signal from spheroids treated with albumin-coated nanoparticles. Albumin-coated beads were incubated with collagenase concentration equivalent to the amount of estimated remaining after particle purification.

protein refers to the small amount of residual protein remaining after nanoparticle purification. Dynamic light scattering confirmed that particle size differences between albumin-coated and collagenase-coated nanoparticles were negligible with measured sizes of 110 (±1.2) nm for albumin-coated and 115 (±1.7) nm for collagenase-coated nanoparticles.

Discussion

Our previous work along with other reports in the literature have demonstrated that many nanoparticle-based systems for cancer therapy have limited accumulation in tumor areas, in large part due to inefficient tumor penetration (Yuan et al 1994; Graff et al 2004; Pun et al 2004). The limited transport of therapeutic small molecules and macromolecules and resulting inaccessibility to most target cells has been identified as a key barrier to drug efficacy (Jain 2001; Tannock et al 2002; Hicks et al 2003). Thus, the diffusion of inert macromolecular tracers such as dextran and albumin with sizes up to ~10 nm has been investigated in collagen gels and solid tumors in vivo (Nugent and Jain 1984; Ramanujan et al 2002; Dreher et al 2006). However, to our knowledge, a systematic study of larger nanoparticles and the effect of ECM integrity has not been reported. This work investigates nanoparticle (20–200 nm in diameter) penetration and the effect of ECM integrity in a three-dimensional spheroid model.

Fluorescently-labeled, polystyrene beads were used as model nanoparticles for these studies because they are spherical in shape, as are many nanoparticulate delivery vehicles, and they can be obtained in a range of sizes. Carboxylate polystyrene beads were chosen because the particles can be readily conjugated to targeting ligands for future studies (Popielarski et al 2005). The negatively-charged beads are also expected to have reduced non-specific binding of cells, which contain a number of negatively-charged membrane components such as proteoglycans (Mislick and Baldeschwieler 1996), although non-specific adsorption of proteins from the media could significantly alter the surface properties on the nanoparticles once they are added to cell cultures. Previous work has shown that the "binding barrier" resulting from high affinity binding of particles to tissue sites immediately after extravasation prevents diffusion into deeper tissue (Juweid et al 1992; Graff and Wittrup 2003). Nanoparticle penetration was assessed in a three-dimensional multicellular spheroid (MCS) model. This model was chosen because the MCS can be grown under controlled conditions with good reproducibility and homogeneity. MCS are also known to produce ECM and to pack with physiologically-relevant gradients of nutrient accessibility and cell growth rates. As a result, MCS have been a valuable model in drug penetration studies (Sutherland 1988).

One major focus in this study was the effect of ECM degradation on nanoparticle delivery. Collagenase treatment conditions were optimized and the collagen distribution in MCS was assessed before and after collagenase treatment. Spheroids were treated with 0.1 mg/ml of collagenase for 5 h because the kinetics of collagen degradation with 1.0 mg/ml collagenase was found to be on the order of a few hours (Brown et al 2003). In order to retain spheroid integrity with a gentler treatment, a lower collagenase concentration over a longer time was applied. Collagen staining showed a relatively uniform distribution throughout the spheroid. After collagenase treatment, very low amounts of collagen were detected, especially in the spheroid periphery.

Nanoparticle penetration into the spheroids was limited for all particle sizes tested in the absence of collagenase treatment; most nanoparticles remained concentrated at the spheroid rim. Although 20 nm and 40 nm nanoparticles showed some penetration into the core, this penetration was still below 60% of the total spheroid associated nanoparticles. This means that the outer cell layers, which represent a small portion of the overall volume, contain at least 40% of associated nanoparticles. These smaller nanoparticles may have transport access because they are small enough to diffuse between organized collagen fibrils. The spacing of these fibrils in tumors has been measured to be 20–40 nm, although, larger interfibrillar spacing (75–130 nm) was observed in poorly-organized tumor ECM (Pluen et al 2001). The spheroid model used here was relatively tight packed.

Collagenase treatment increased delivery efficiency for 20, 40, and 100 nm particles. The 20 nm nanoparticles are

affected to a lesser extent than 40 nm particles because the 20 nm particles are better able to diffuse within the spheroid in the absence of collagenase. Little improvement in particle penetration was observed for particles with diameters above 100 nm. Collagenase treatment appears to remove most diffusional restrictions for the 40 nm particles although transport of the 100 nm particles into the spheroid is improved only slightly.

Collagen fiber degradation likely increases the accessible space in the spheroids for nanoparticle transport, defined as the available volume fraction (K_v) (Krol et al 1999; Yuan et al 2001). An increase in K_v can improve nanoparticle penetration by increasing pore size to allow access of larger particles and decreasing frictional resistance to diffusion through the pores, by increasing pore connectivity, or by reducing torturosity. The importance of these parameters in effective drug delivery has been well-covered in the literature (Krol et al 1999; Yuan et al 2001; Ramanujan et al 2002).

Upregulated collagenase levels have been associated with more aggressive tumors because metalloprotease activity is used by migrating and invading cells (Rao et al 2005; Xu et al 2005). Therefore, systemic collagenase co-treatment and direct injection of collagenase with nanoparticles into tumor carries risk due to possible differences in the biodistribution of the free enzyme and the nanoparticle, leading to a temporal and spatial difference in delivery of the two components to the tumor. A more attractive approach is to immobilize the collagenase with the nanoparticle to ensure co-delivery. To this end, collagenase was immobilized on nanoparticle surfaces by adsorption. Collagenase activity was retained by the adsorbed protein, and delivery of collagenase-coated, 100 nm nanoparticles with active collagenase increases particle penetration by 4-fold compared with albumin-coated nanoparticles. These preliminary results suggest that a nanoparticle delivery system, with proper targeting to tumor tissue, could result in local delivery of active collagenase leading to increased penetration of delivered therapeutics.

The results presented here provide information that would be useful for the design of nanoparticle carriers for delivery to solid tumors. Carriers 100 nm or larger will likely experience a high amount of exclusion from tumor tissue, although the surface properties of the particle will most likely have a significant effect on penetration into the tumor tissue and warrants further investigation. Reduction of collagen in the extracellular matrix can reduce the hindrance of previously excluded 100 nm particles, and even increase the local concentration of smaller particles that are initially relatively free to diffuse in tumor tissue. Transmission electron microscopy revealed that, despite the presence of a number of large pores between cells, which offer a plausible route for particle diffusion, a significant number of tight junctions between cells in the SiHa MCS model still remain. Therefore, the use of molecules to modify tight junctions may result in similar increases in particle penetration to those observed with modulation of collagen and may act synergistically with ECM-modulating approaches. The covalent conjugation of ECM modulating enzymes to therapeutic agents may offer a more stable and versatile option compared with adsorption. Recent studies have shown that nanoparticles containing covalently linked collagenase on their surfaces exhibit improved penetration in collagen gels (Kuhn et al 2006). Future studies will focus on extending this work beyond model nanoparticles to therapeutically relevant nanoparticles and incorporation of ECM and/or tight junction-modifying molecules into the delivery vehicle for targeted delivery of penetration enhancing agents.

Acknowledgments

Grant Support: NIH/NCI grant 1R21CA114141-01, the Alliance for Cancer Gene Therapy (SHP, Young Investigator Award), and the National Science Foundation (TTG, Graduate Fellowship). We thank Susan MacPhail for her technical assistance and advice.

References

Alexandrakis G, Brown EB, Tong RT, et al. 2004. Two-photon fluorescence correlation microscopy reveals the two-phase nature of transport in tumors. *Nature Medicine*, 10:203–207.

Brown E, McKee T, diTomaso E, et al. 2003. Dynamic imaging of collagen and its modulation in tumors in vivo using second-harmonic generation. *Nature Medicine*, 9:796–800.

Choi J, Credit K, Henderson K, et al. 2006. Intraperitoneal immunotherapy for metastatic ovarian carcinoma: Resistance of intratumoral collagen to antibody penetration. *Clinical Cancer Research*, 12:1906–1912.

Davies CD, Berk DA, Pluen A, et al. 2002. Comparison of IgG diffusion and extracellular matrix composition in rhabdomyosarcomas grown in mice versus in vitro as spheroids reveals the role of host stromal cells. *British Journal of Cancer*, 86:1639–1644.

Davies CD, Engesaeter BO, Haug I, et al. 2001. Uptake of IgG in osteosarcoma correlates inversely with interstitial fluid pressure, but not with interstitial constituents. *British Journal of Cancer*, 85:1968–1977.

Dreher MR, Liu WG, Michelich CR, et al. 2006. Tumor vascular permeability, accumulation, and penetration of macromolecular drug carriers. *Journal of the National Cancer Institute*, 98:335–344.

Eikenes L, Bruland OS, Brekken C, et al. 2004. Collagenase increases the transcapillary pressure gradient and improves the uptake and distribution of monoclonal antibodies in human osteosarcoma xenografts. *Cancer Research*, 64:4768–4773.

Eikenes L, Tari M, Tufto I, et al. 2005. Hyaluronidase induces a transcapillary pressure gradient and improves the distribution and uptake of liposomal doxorubicin (Caelyx (TM)) in human osteosarcoma xenografts. *British Journal of Cancer*, 93:81–88.

Flessner MF, Choi J, Credit K, et al. 2005. Resistance of tumor interstitial pressure to the penetration of intraperitoneally delivered antibodies into metastatic ovarian tumors. *Clinical Cancer Research*, 11:3117–3125.

Graff BA, Vangberg L, Rofstad EK. 2004. Quantitative assessment of uptake and distribution of iron oxide particles (NC100150) in human melanoma xenografts by contrast-enhanced MRI. *Magnetic Resonance in Medicine*, 51:727–735.

Graff CP, Wittrup KD. 2003. Theoretical analysis of antibody targeting of tumor spheroids: Importance of dosage for penetration, and affinity for retention. *Cancer Research*, 63:1288–1296.

Grantab R, Sivananthan S, Tannock IF. 2006. The penetration of anticancer drugs through tumor tissue as a function of cellular adhesion and packing density of tumor cells. *Cancer Research*, 66:1033–1039.

Grill J, Lamfers MLM, van Beusechem VW, et al. 2002. The organotypic multicellular spheroid is a relevant three-dimensional model to study adenovirus replication and penetration in human tumors in vitro. *Molecular Therapy*, 6:609–614.

Hicks KO, Pruijn FB, Sturman, JR, et al. 2003. Multicellular resistance to tirapazamine is due to restricted extravascular transport: A pharmacokinetic/pharmacodynamic study in HT29 multicellular layer cultures. *Cancer Research*, 63:5970–5977.

Jain RK. 2001. Delivery of molecular and cellular medicine to solid tumors. *Advanced Drug Delivery Reviews*, 46:149–168.

Juweid M, Neumann R, Paik C, et al. 1992. Micropharmacology of Monoclonal-Antibodies in Solid Tumors - Direct Experimental-Evidence for a Binding-Site Barrier. *Cancer Research*, 52:5144–5153.

Kaul G, Amiji M. 2005. Tumor-targeted gene delivery using poly(ethylene glycol)-modified gelatin nanoparticles: In vitro and in vivo studies. *Pharmaceutical Research*, 22:951–961.

Kostarelos K, Emfietzoglou D, Papakostas A, et al. 2004. Binding and interstitial penetration of liposomes within avascular tumor spheroids. *International Journal of Cancer*, 112:713–721.

Krol A, Maresca J, Dewhirst MW, et al.1999. Available volume fraction of macromolecules in the extravascular space of a fibrosarcoma: Implications for drug delivery. *Cancer Research*, 59:4136–4141.

Kuhn SJ, Finch SK, Hallahan DE, et al. 2006. Proteolytic surface functionalization enhances in vitro magnetic nanoparticle mobility through extracellular matrix. *Nano Letters*, 6:306–312.

Kuppen PJK, van der Eb MM, Jonges LE, et al. 2001. Tumor structure and extracellular matrix as a possible barrier for therapeutic approaches using immune cells or adenoviruses in colorectal cancer. *Histochemistry and Cell Biology*, 115:67–72.

Kuriyama N, Kuriyama H, Julin CM, et al. 2001. Protease pretreatment increases the efficacy of adenovirus-mediated gene therapy for the treatment of an experimental glioblastoma model. *Cancer Research*, 61:1805–1809.

McKee TD, Grandi P, Mok W, et al. 2006. Degradation of fibrillar collagen in a human melanoma xenograft improves the efficacy of an oncolytic herpes simplex virus vector. *Cancer Research*, 66:2509–2513.

Mislick KA, Baldeschwieler JD. 1996. Evidence for the role of proteoglycans in cation-mediated gene transfer. *Proceedings of the National Academy of Sciences of the United States of America*, 93:12349–12354.

Moghimi SM, Hunter AC, Murray JC. 2001. Long-circulating and target-specific nanoparticles: Theory to practice. *Pharmacological Reviews*, 53:283–318.

Netti PA, Berk DA, Swartz MA, et al. 2000. Role of extracellular matrix assembly in interstitial transport in solid tumors. *Cancer Research*, 60:2497–2503.

Nugent LJ, Jain RK. 1984. Extravascular Diffusion in Normal and Neoplastic Tissues. *Cancer Research*, 44:238–244.

O'Neal DP, Hirsch LR, Halas NJ, et al. 2004. Photo-thermal tumor ablation in mice using near infrared-absorbing nanoparticles. *Cancer Letters*, 209:171–176.

Oloumi A, MacPhail SH, Johnston PJ, et al. 2000. Changes in Subcellular Distribustion of Topoisomerase IIα Correlate with Etoposide Resistance in Multicellular Spheroids and Xenograft Tumors. *Cancer Research*, 60: 5747–5753.

Pluen A, Boucher Y, Ramanujan S, et al. 2001. Role of tumor-host interactions in interstitial diffusion of macromolecules: Cranial vs. subcutaneous tumors. *Proceedings of the National Academy of Sciences of the United States of America*, 98:4628–4633.

Popielarski SR, Pun SH, Davis ME. 2005. A nanoparticle-based model delivery system to guide the rational design of gene delivery to the liver. 1. Synthesis and characterization. *Bioconjugate Chemistry*, 16:1063–1070.

Portney NG, Ozkan M. 2006. Nano-oncology: drug delivery, imaging, and sensing. *Analytical and Bioanalytical Chemistry*, 384:620–630.

Pun SH, Tack F, Bellocq NC, et al. 2004. Targeted delivery of RNA-cleaving DNA enzyme (DNAzyme) to tumor tissue by transferrin-modified, cyclodextrin-based particles. *Cancer Biology & Therapy*, 3:641–650.

Ramanujan S, Pluen A, McKee TD, et al. 2002. Diffusion and convection in collagen gels: Implications for transport in the tumor interstitium. *Biophysical Journal*, 83:1650–1660.

Rao JS, Gondi C, Chetty C, et al. 2005. Inhibition of invasion, angiogenesis, tumor growth, and metastasis by adenovirus-mediated transfer of antisense uPAR and MMP-9 in non-small cell lung cancer cells. *Molecular Cancer Therapeutics*, 4:1399–1408.

Sutherland RM. 1988. Cell and Environment Interactions in Tumor Microregions - the Multicell Spheroid Model. *Science*, 240:177–184.

Tannock IF, Lee CM, Tunggal JK, et al. 2002. Limited penetration of anticancer drugs through tumor tissue: A potential cause of resistance of solid tumors to chemotherapy. *Clinical Cancer Research*, 8:878–884.

Vanderrest M, Cole WG, Glorieux FH. 1977. Human Collagen Fingerprints Produced by Clostridiopeptidase-a Digestion and High-Pressure Liquid-Chromatography. *Biochemical Journal*, 161:527–534.

Xu XP, Wang Y, Chen ZH, et al. 2005. Matrix metalloproteinase-2 contributes to cancer cell migration on collagen. *Cancer Research*, 65:130–136.

Yuan F, Krol A, Tong S. 2001. Available space and extracellular transport of macromolecules: Effects of pore size and connectedness. *Annals of Biomedical Engineering*, 29:1150–1158.

Yuan F, Salehi HA, Boucher Y, et al. 1994. Vascular-Permeability and Microcirculation of Gliomas and Mammary Carcinomas Transplanted in Rat and Mouse Cranial Windows. *Cancer Research*, 54:4564–4568.